Spin current leakage and Onsager reciprocity in interfacial spin-charge interconversion

Aurélien Manchon [1,*] Shuyuan Shi,[2,3] and Hyunsoo Yang[2]

[1]*Aix-Marseille Université, CNRS, CINaM, Marseille, France*
[2]*Department of Electrical and Computer Engineering, National University of Singapore, Singapore 117576, Singapore*
[3]*Fert Beijing Institute, MIIT Key Laboratory of Spintronics, School of Integrated Circuit Science
and Engineering, Beihang University, Beijing 100191, China*

Experimental investigations of spin-charge interconversion in magnetic bilayers comprising a ferromagnet adjacent to a topological insulator have reported scattered results on the spin-charge and charge-spin conversion efficiency. Attempting to reconcile these contradicting experimental results, we develop a phenomenological theory of spin-charge interconversion accounting for both interfacial interconversion through the spin galvanic effect, also called the Rashba-Edelstein effect, as well as bulk interconversion via the spin Hall effect. We find that the spin current leakage into the nonmagnetic metal plays a central role during the spin-to-charge and charge-to-spin conversion, leading to dissymmetric interconversion processes. In particular, spin-to-charge conversion is much less sensitive to the spin current absorption in the nonmagnetic metal than charge-to-spin conversion. This suggests that spin pumping is a more trustable technique to extract the interfacial Rashba parameter than spin-orbit torque.

I. INTRODUCTION

Spin-to-charge interconversion mediated by spin-orbit coupling has become a central technique in spintronics enabling the electrical manipulation of magnetization [1], as well as the generation of charge currents induced by magnetization precession [2–4]. The standard system is composed of a magnetic thin film deposited on top of a nonmagnetic metal with strong spin-orbit coupling. Whereas the original workhorse of spin-charge interconversion was NiFe/Pt [5], a broad range of materials has been explored over the years, including both metallic [6–8] and insulating ferromagnets [9–12] and antiferromagnets [13,14] adjacent to strongly spin-orbit coupled materials including transition metals (Pt, W, and Ta). In these systems, the interconversion is mostly attributed to the spin Hall effect (SHE) taking place in the bulk of the heavy metal [15,16]. In the past decade, attention has been shifted toward materials displaying large interfacial spin-momentum locking. Recent research encompasses metals with strong interfacial Rashba states [17–19] (Ag/Bi, Ag/Sb or Ag/Bi$_2$O$_3$), topological insulators [20–33] (Bi$_2$Se$_3$, etc.), transition metal dichalcogenides [34–38] (MoS$_2$, WTe$_2$), van der Waals materials [39–43] (for nonlocal interconversion, see Refs. [44,45]), oxide heterostructures [46–50] (see Ref. [51] for a review), chiral metals [52], and the so-called ferroelectric Rashba semiconductors such as SrTiO$_3$ and α-GeTe [53,54], whose interfacial spin-momentum locking can be controlled by switching the ferroelectric polarization [55].

In all these materials, strong spin-orbit coupling and inversion symmetry breaking at the interface result in Dirac or Rashba spin-momentum locking [56], which enables interconversion between charge and spin currents via the so-called (inverse) spin galvanic effect (SGE), also known as the Rashba-Edelstein effect [57–59]. In contrast to the SHE that converts three-dimensional (3D) spin currents into 3D charge currents, the interfacial spin galvanic effect converts a two-dimensional (2D) charge current into a 3D spin current, and vice-versa. The interconversion efficiency of SHE is quantified by the dimensionless parameters ξ_{cs} and ξ_{sc}. In a bulk heavy metal, Onsager reciprocity dictates that $\xi_{cs} = \xi_{sc}$. As discussed in more detail in the present work, in the case of a magnetic bilayer, this equality holds true only when neglecting interfacial conversion and provided that the nonmagnetic metal is a good spin insulator.

The interconversion efficiency of SGE is rather quantified in terms of spin-to-charge conversion length λ_{sc} and charge-to-spin conversion inverse length q_{cs}. From a theoretical standpoint, ξ is related to the SHE in the bulk heavy metal modulated by the spin transparency, i.e., the ability of the heavy metal to absorb the spin current. The figures of merit λ_{sc} and q_{cs} have been recently derived for a 2D Rashba or Dirac gas in Refs. [33,60–62] using either phenomenological or microscopic approaches. These references provide the general form $\lambda_{sc} = (\alpha_R/\hbar)(1/\tau_p + 1/\tau_t)$ and $q_{cs} = (\alpha_R/\hbar v_F^2)\tau_t$, where τ_t is the tunneling time between the 2D gas and the spin current source (typically an adjacent ferromagnet, but also possibly a nonmagnetic metal through which the spin current is injected) and τ_p is the momentum relaxation time in the 2D gas. We emphasize that the validity of these theories, as well as the very definition of λ_{sc} and q_{cs}, is restricted to the ideal case of 2D transport. In other words, whereas these parameters are meaningful in the case of oxide heterostructures where the charge current is purely two-dimensional, it may simply
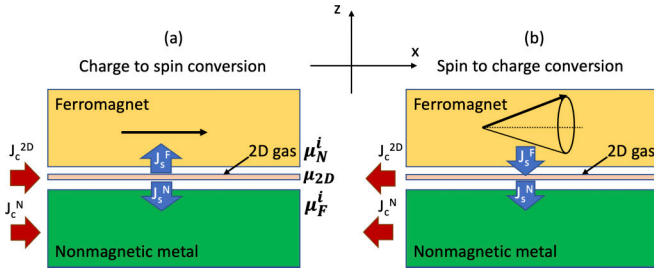
*aurelien.manchon@univ-amu.fr

FIG. 1. (a) Charge-to-spin and (b) spin-to-charge conversion in a metallic bilayer composed of a 2D gas embedded between a ferromagnet and a nonmagnetic metal.

not apply in other metallic systems or in weakly insulating "topological insulators" such as Bi_2Se_3.

As a matter of fact, experiments in topological insulators report large variations in spin-charge interconversion efficiency. In particular, it is often observed that spin-to-charge and charge-to-spin conversion efficiencies massively differ from each other. Charge-to-spin conversion in Bi-based topological materials ranges from 0.4 to more than 400 [20,21,23,24,27,29–31] whereas spin-to-charge conversion rather ranges from 0.0001 to 0.4 [22,23,25,26], which cannot be properly accounted for using the simple formulas given above. This set of results contrasts sharply with the metallic case, where the reported efficiencies, ξ_{cs} and ξ_{sc}, are usually of the same order.

In an attempt to clarify the situation, we develop a phenomenological model for spin-charge interconversion in a metallic bilayer where interfacial SGE and bulk SHE coexist. We show that whereas spin-to-charge and charge-to-spin conversion are intrinsically asymmetric, although not breaking Onsager reciprocity, the leakage of the spin current in the neighboring nonmagnetic metal plays a crucial role when the conductivity of the nonmagnetic metal becomes large.

II. DRIFT-DIFFUSION THEORY

We consider the system represented in Fig. 1 and composed of three elements: a 2D gas embedded between a ferromagnet F and a nonmagnetic metal N, of thicknesses d_F and d_N, respectively. The 2D gas can be thought of as the surface state of a heavy metal (e.g., Co/Pt, Ag/Bi) or that of a weakly conductive topological insulator (e.g., Bi_2Se_3). For simplicity, we assume that the spin-charge conversion in the 2D gas takes place through the SGE (or Rashba-Edelstein) effect, with an effective coupling α_R (eV m), and in the nonmagnetic metal, it is induced by SHE with an angle θ_H (unitless),

$$\mathbf{J}_c^{2D} = \sigma_{2D}\mathbf{E} - e^2 \mathcal{N}_{2D} \frac{\alpha_R}{\hbar} \mathbf{z} \times \boldsymbol{\mu}_{2D}, \quad (1)$$

where the second term is the SGE that converts a nonequilibrium spin density into a charge current. Here, $\boldsymbol{\mu}_{2D} = \mu_{2D}\mathbf{y}$ (in the units of V) is the spin chemical potential, $\mathcal{N}_{2D}$ (eV^{-1} m^{-2}) and σ_{2D} (Ω^{-1}) are the density of states and conductivity of the 2D gas. The spin continuity equation reads

$$\partial_t \boldsymbol{\mu}_{2D} = \frac{\alpha_R}{\hbar}\mathbf{z} \times \mathbf{E} - \frac{\boldsymbol{\mu}_{2D}}{\tau_{sf}} - \frac{\boldsymbol{\mu}_{2D} - \boldsymbol{\mu}_F^i}{\tau_F} - \frac{\boldsymbol{\mu}_{2D} - \boldsymbol{\mu}_N^i}{\tau_N}. \quad (2)$$

The first term is the inverse SGE, i.e., the generation of a spin density induced by the flow charge, with α_R being the so-called Rashba parameter. A formal derivation of the spin diffusion equation in a Rashba gas can be found in Refs. [63–65]. The second term accounts for the spin relaxation in the interfacial gas (that may be anisotropic, although for the sake of simplicity, this is neglected in the present study) and the last two terms account for spin injection in the neighboring layers: $1/\tau_{F(N)}$ is the tunneling rate between the 2D gas and the ferromagnet (nonmagnetic metal), and $\boldsymbol{\mu}_{F(N)}^i$ is the interfacial spin chemical potential in the ferromagnet (nonmagnetic metal). These tunneling rates are related to the interfacial spin currents flowing between the 2D gas and the ferromagnetic ($\mathbf{J}_s^{F,i}$) and nonmagnetic metals ($\mathbf{J}_s^{N,i}$) through the boundary conditions

$$\mathbf{J}_s^{N,i} = G_N(\boldsymbol{\mu}_N^i - \boldsymbol{\mu}_{2D}), \quad (3)$$

where $G_N = e^2 \mathcal{N}_{2D}/\tau_N$ (Ω^{-1} m^{-2}) is the interfacial conductance between the 2D gas and the nonmagnetic metal. Notice that without loss of generality, the spin current is expressed in the same units as the charge current for simplicity. Similarly,

$$\mathbf{J}_s^{F,i} = 2G_{\uparrow\downarrow}\boldsymbol{\mu}_{2D} - \mathbf{J}_s^0, \quad (4)$$

where $\mathbf{J}_s^0$ is due to spin pumping (if any), and $2G_{\uparrow\downarrow} = e^2 \mathcal{N}_{2D}/\tau_F$ is the spin mixing conductance (Ω^{-1} m^{-2}), assuming that the magnetization is perpendicular to the spin density in the 2D gas (which is valid in both spin-to-charge and charge-to-spin interconversion scenarios), i.e., $\mu_F^i = 0$.

In the nonmagnetic metal, the (3D) charge and spin currents, $\mathbf{J}_c^N$ and $\mathbf{J}_s^N$, are defined

$$\mathbf{J}_c^N = \sigma_N\mathbf{E} + \theta_H\sigma_N\boldsymbol{\nabla} \times \boldsymbol{\mu}_N, \quad (5)$$

$$\mathbf{J}_s^N = -\sigma_N\boldsymbol{\nabla}\boldsymbol{\mu}_N - \theta_H\sigma_N\mathbf{y} \times \mathbf{E}. \quad (6)$$

Here, one recognizes the SHE and inverse SHE, σ_N (Ω^{-1} m^{-1}) being the conductivity of the metal. In the scenario studied in the present work, the spin polarization remains aligned along $\mathbf{y}$ and therefore all the equations above can be simply projected along this direction. Applying the two boundary conditions $J_s^N(z = 0) = G_N(\mu_N^i - \mu_{2D})$ and $J_s^N(z = -d_N) = 0$, we obtain

$$\mu_N(z) = \frac{1}{1 + \eta_N}(\eta_N\mu_{2D} + \tilde{\lambda}_N\tilde{\theta}_H E)\frac{\cosh\frac{z+d_N}{\lambda_N}}{\cosh\frac{d_N}{\lambda_N}}$$

$$+ \tilde{\lambda}_N\tilde{\theta}_H E \frac{\tanh\frac{d_N}{\lambda_N}\sinh\frac{z}{\lambda_N}}{\cosh\frac{d_N}{\lambda_N} - 1}, \quad (7)$$

where $\tilde{\theta}_H = \theta_H(1 - \cosh^{-1}\frac{d_N}{\lambda_N})$, $\tilde{\lambda}_N = \lambda_N/\tanh\frac{d_N}{\lambda_N}$, and $\eta_N = \tilde{\lambda}_N G_N/\sigma_N$. The coefficient $1/(1 + \eta_N)$ quantifies the spin current backflow from the nonmagnetic metal. Indeed, if the nonmagnetic metal is a perfect spin insulator (long spin diffusion length), $1/(1 + \eta_N) \to 0$. In the case of spin pumping, $E = 0$, and the spin current backflow exactly compensates the pumped spin current at the interface, leading to $\mu_N^i = \mu_{2D}$. In the opposite case, when the nonmagnetic metal is a perfect spin sink (very short spin diffusion length), $1/(1 + \eta_N) \to 1$ and the spin current backflow vanishes, leading to $\mu_N^i = 0$. Let us now compute the spin-charge interconversion efficiency in the cases depicted in Fig. 1.

A. Charge-to-spin conversion

An electric field **E** is applied along **x** and generates a spin accumulation, polarized along **y**, throughout the structure [see Eq. (7)]. This spin accumulation injects a spin current $J_s^{F,i}$ into the ferromagnet. In the absence of spin pumping, $J_s^{F,i} = 2G_{\uparrow\downarrow}\mu_{2D}$ [Eq. (4)]. The spin chemical potential μ_{2D} can be obtained from the spin continuity equation, Eq. (2), posing $\partial_t \mu_{2D} = 0$ and injecting $\mu_N^i = \mu_N(0)$ [Eq. (7)]. We get

$$\mu_{2D} = \frac{\frac{\alpha_R}{\hbar} + \frac{1}{\tau_N}\frac{\tilde{\lambda}_N \tilde{\theta}_H}{1+\eta_N}}{\frac{1}{\tau_{sf}} + \frac{1}{\tau_F} + \frac{1}{\tau_N}\frac{1}{1+\eta_N}} E, \tag{8}$$

which implies that

$$J_s^{F,i} = 2G_{\uparrow\downarrow} \frac{\frac{\alpha_R}{\hbar} + \frac{1}{\tau_N}\frac{\tilde{\lambda}_N \tilde{\theta}_H}{1+\eta_N}}{\frac{1}{\tau_{sf}} + \frac{1}{\tau_F} + \frac{1}{\tau_N}\frac{1}{1+\eta_N}} E. \tag{9}$$

To obtain the unitless charge-to-spin interconversion efficiency, we divide the spin current by the current flowing in both the nonmagnetic metal and 2D gas, $J_c = \frac{\sigma_N d_N + \sigma_{2D}}{d_N + t_{2D}}E$, where t_{2D} is the effective thickness of the 2D gas. We then obtain

$$\xi_{cs} = \left| \frac{J_s^{F,i}}{J_c} \right| = 2G_{\uparrow\downarrow} \frac{d_N + t_{2D}}{\sigma_N d_N + \sigma_{2D}} \frac{\frac{\alpha_R}{\hbar} + \frac{1}{\tau_N}\frac{\tilde{\lambda}_N \tilde{\theta}_H}{1+\eta_N}}{\frac{1}{\tau_{sf}} + \frac{1}{\tau_F} + \frac{1}{\tau_N}\frac{1}{1+\eta_N}}. \tag{10}$$

One immediately notices the competition between the spin relaxation inside the 2D gas ($\sim 1/\tau_{sf}$) and the spin absorption in the nonmagnetic metal ($\sim 1/\tau_N$) and in the ferromagnet ($\sim 1/\tau_F \propto G_{\uparrow\downarrow}$). This competition will be analyzed in more detail in the next section. For now, we emphasize that other renormalizations can be adopted. For instance, assuming that the charge-to-spin conversion only occurs in the 2D gas ($\theta_H = 0$), one can normalize the spin current to the charge current that effectively flows along the interface, $J_c^{2D} = \sigma_{2D}E$, which yields

$$q_{cs} = \left| \frac{J_s^{F,i}}{J_c^{2D}} \right| = \frac{\alpha_R}{\hbar} \frac{2G_{\uparrow\downarrow}}{\sigma_{2D}} \frac{1}{\frac{1}{\tau_{sf}} + \frac{1}{\tau_F} + \frac{1}{\tau_N}\frac{1}{1+\eta_N}}. \tag{11}$$

This expression extends the ones derived in Refs. [33,60–62] beyond the model Rashba or Dirac gas, and includes the effect of the adjacent spin sink, providing a more accurate expression for the figure of merit of interfacial charge-to-spin conversion.

B. Spin-to-charge conversion

A spin current $J_s^{F,i} = -(e^2 \mathcal{N}_{2D})/\tau_F \mu_{2D} + J_s^0$ is pumped out of the ferromagnet and converted into a charge current composed of $J_c^{2D} = e^2 \mathcal{N}_{2D}(\alpha_R/\hbar)\mu_{2D}$ and $J_c^N = -(1/d_N)\int_{-d_N}^0 dz \theta_H \sigma_N \partial_z \mu_N$. The spin continuity equation, Eq. (2), gives

$$\mu_{2D} = \frac{J_s^0}{e^2 \mathcal{N}_{2D}} \frac{1}{\frac{1}{\tau_{sf}} + \frac{1}{\tau_F} + \frac{1}{\tau_N}\frac{1}{1+\eta_N}}. \tag{12}$$

Therefore, we deduce the charge current flowing in the 2D gas and in the nonmagnetic metal,

$$J_c^{2D} = \frac{\alpha_R}{\hbar} \frac{1}{\frac{1}{\tau_{sf}} + \frac{1}{\tau_F} + \frac{1}{\tau_N}\frac{1}{1+\eta_N}} J_s^0, \tag{13}$$

$$J_c^N = \frac{\tilde{\theta}_H \tilde{\lambda}_N}{d_N} \frac{1}{\frac{1}{\tau_{sf}} + \frac{1}{\tau_F} + \frac{1}{\tau_N}\frac{1}{1+\eta_N}} J_s^0. \tag{14}$$

The total current that is pumped through the system is therefore $I_c^{pump} = w(J_c^N d_N + J_c^{2D})$. In other words, if the effective {nonmagnetic + 2D gas} thickness is $d_N + t_{2D}$, the effective current density pumped out of the system is $J_c^{pump} = (J_c^N d_N + J_c^{2D})/(d_N + t_{2D})$. Finally, the spin-to-charge efficiency reads

$$\xi_{sc} = \left| \frac{J_c^{pump}}{J_s^{F,i}} \right| = \frac{1}{d_N + t_{2D}} \frac{\frac{\alpha_R}{\hbar} + \frac{1}{\tau_N}\frac{\tilde{\lambda}_N \tilde{\theta}_H}{1+\eta_N}}{\frac{1}{\tau_{sf}} + \frac{1}{\tau_N}\frac{1}{1+\eta_N}}. \tag{15}$$

Equations (10) and (15) are the central results of this work. They account for charge-to-spin and spin-to-charge conversion efficiencies in the presence of *both* interfacial and bulk spin-charge interconversion. One immediately sees that, besides an obvious geometrical factor, these expressions differ on the role played by the spin mixing conductance, $G_{\uparrow\downarrow} \propto 1/\tau_F$, so that in general $\xi_{cs} \neq \xi_{sc}$. As discussed below, they are only equal in the absence of interfacial spin-charge interconversion, when the ferromagnet is strongly coupled to the nonmagnetic metal.

Notice though that this inequality does not mean that Onsager reciprocity is broken at all. As a matter of fact, Onsager reciprocity applies to the response tensor of generalized currents to thermodynamical forces, or, in other words, to the connection between current densities and chemical potential gradients (for a discussion on Onsager reciprocity applied to spin pumping and spin torque, see Ref. [66]). Since the spin-charge interconversion efficiencies are defined as the ratio between two current densities, they do not fulfill Onsager reciprocity.

In fact, two limits illustrate the difference between spin-to-charge and charge-to-spin conversion in metallic bilayers. Let us first assume that the interfacial spin-charge interconversion is absent, i.e., $G_N \to +\infty$, $t_{2D} \to 0$, $\sigma_{2D} \to 0$, and $\tau_{sf} \to +\infty$. When the ferromagnet is directly coupled to the nonmagnetic metal, $2G_{\uparrow\downarrow}\tilde{\lambda}_N/\sigma_N \gg 1$, we obtain

$$\xi_{sc} = \frac{\tilde{\lambda}_N}{d_N}\tilde{\theta}_H \approx \xi_{cs} = \tilde{\theta}_H. \tag{16}$$

On the contrary, assuming only interfacial spin-to-charge conversion is allowed, the charge current is entirely pumped into the 2D gas and the spin-to-charge conversion length reads

$$\lambda_{sc} = \frac{\alpha_R}{\hbar} \frac{1}{\frac{1}{\tau_{sf}} + \frac{1}{\tau_N}\frac{1}{1+\eta_N}}, \tag{17}$$

which qualitatively agrees with the expressions derived in Refs. [33,60–62]. The difference is that in Eq. (17), the momentum relaxation time τ_p is replaced by the spin-flip time in the 2D gas τ_{sf}, and the tunneling time τ_t is replaced by τ_N, accounting for the backflow spin current in the nonmagnetic metal.
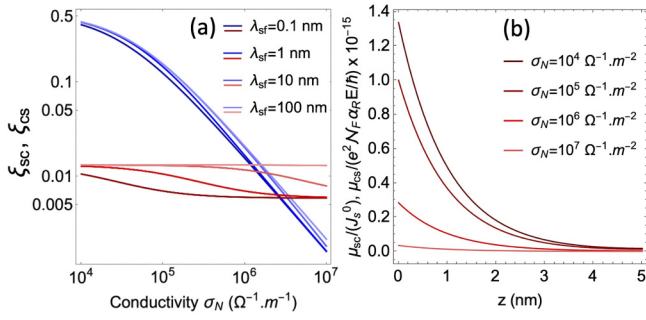
FIG. 2. (a) Spin-to-charge (red) and charge-to-spin (blue) conversion efficiency as a function of the conductivity of the nonmagnetic metal for different values of the spin diffusion length λ_N. (b) Spin accumulation profile in the nonmagnetic metal for different values of the conductivity σ_N. In these calculations, we set $\tau_{sf} = 10^{-14}$ s, $\sigma_{2D} = 2 \times 10^{-4}$ Ω^{-1}, $d_N = 5$ nm, and $t_{2D} = 1$ nm.

III. INFLUENCE OF SPIN CURRENT LEAKAGE

A. Phenomenological parameters

Besides the conventional electronic properties of the metallic layers (conductivity, spin diffusion length, spin Hall angle), the phenomenological theory developed in the previous section is controlled by two parameters: the coupling between the ferromagnetic layer and the 2D gas, $1/\tau_F = 2G_{\uparrow\downarrow}/e^2\mathcal{N}_F$, and the coupling between the 2D gas and the nonmagnetic metal, $1/\tau_N = G_N/e^2\mathcal{N}_N$. Qualitatively, the interfacial areal conductance between two metallic layers is about $e^2/hA \approx 10^{14}$–10^{15} Ω^{-1} m^{-2} (see, e.g., Refs. [67,68]), A being the area of a unit cell at the interface. Assuming an interfacial density of state of about $1/(eV\,A)$, one arrives at a coupling rate of $1/\tau_{N,F} \approx 10^{15}$ s^{-1}, which seems reasonable for direct coupling between metallic states and remains one to two orders of magnitude larger than the typical spin relaxation rate in metals.

B. Interfacial interconversion

Let us first consider the case where the spin-charge interconversion is solely due to spin-momentum locking at the interface. In this case, the adjacent metallic layer does not participate to the conversion itself but only in the spin absorption. To model this case, we set the following parameters, $G_N = 2G_{\uparrow\downarrow} = 4 \times 10^{14}$ Ω^{-1} m^{-2}. In Fig. 2(a), we report the dependence of the interconversion efficiencies, ξ_{sc} (red) and ξ_{cs} (blue), as a function of the nonmagnetic metal conductivity σ_N for various values of the spin diffusion length λ_N. Notice that the figure is given in logarithmic scale. Clearly, the spin-to-charge and charge-to-spin conversion efficiencies are markedly different in the limit of weakly conducting nonmagnetic metal ($\sigma_N \approx 10^4$ Ω^{-1} m^{-1}), providing an explanation for the experimental values reported in bilayers involving topological insulators (Bi$_2$Se$_3$, etc.), as pointed out above. Upon increasing the conductivity of the nonmagnetic metal, the charge-to-spin efficiency (blue) is progressively reduced whereas the spin-to-charge efficiency (red) is only weakly affected. This distinct behavior is directly related to the current shunting that strongly affects the charge-to-spin conversion while leaving the spin-to-charge conversion unaffected. In the

case of a conducting nonmagnetic metal ($\sigma_N \approx 10^6$ Ω^{-1} m^{-1}), both efficiencies are comparable, as mentioned in the previous section, corroborating the experimental data collected using a conducting heavy metal substrate such as Pt. Reducing the spin diffusion length reduces the interconversion efficiency, as the spin information is lost in the nonmagnetic metal.

In the model proposed above, the interfacial spin chemical potential due to spin pumping, μ_N^{sc}, and that due to electrical injection, μ_N^{cs}, are related by

$$\frac{\mu_N^{sc}(z)}{J_s^0} = \frac{\mu_N^{cs}(z)}{(e^2\mathcal{N}_F\alpha_R/\hbar)E}, \tag{18}$$

$$= \frac{\eta_N}{1+\eta_N} \frac{\cosh\frac{z+d_N}{\lambda_N}}{\cosh\frac{d_N}{\lambda_N}} \frac{1}{\frac{1}{\tau_{sf}} + \frac{1}{\tau_F} + \frac{1}{\tau_N}\frac{1}{1+\eta_N}}. \tag{19}$$

The profile of the spin chemical potential is reported in Fig. 2(b) for $\lambda_N = 1$ nm and for various conductivities σ_N. The larger the conductivity the smaller the interfacial spin chemical potential, suggesting that interfacial spin-charge interconversion is enhanced when the adjacent layer is a good spin insulator.

C. Interfacial versus bulk interconversion

Let us now turn on the spin Hall angle of the nonmagnetic layer. Figure 3 reports the interconversion efficiencies as a function of the nonmagnetic metal conductivity for various magnitudes of the spin Hall angle and for low [Fig. 3(a)], medium [Fig. 3(b)], and strong value of the Rashba term [Fig. 3(e)]. On the right panel, we show the contribution of SGE (solid) and SHE (dashed) to spin-to-charge (red) and charge-to-spin conversions (blue).

In the case of vanishingly weak Rashba strength [Figs. 3(a) and 3(b)], the interconversion is dominated by the (inverse) SHE and steadily increases with θ_H. The spin-to-charge interconversion efficiency ξ_{sc} (red lines) increases with the conductivity of the normal metal as more output charge current is allowed to flow. On the other hand, the charge-to-spin interconversion efficiency ξ_{cs} (blue lines) decreases in the limit of highly conductive normal metal as the shunting increases. To understand this feature, Fig. 3(b) shows that the contributions of the SGE and ISGE systematically decrease when increasing the conductivity of the nonmagnetic metal, as relatively less current flows inside the 2D gas. Notice that the effect is more dramatic for the spin-to-charge than for the charge-to-spin conversion. The contribution of the SHE is more subtle. Whereas its contribution to the charge-to-spin interconversion increases steadily (dashed red), its contribution to spin-to-charge interconversion first increases, reaches a maximum, and then decreases (dashed blue). This behavior is associated with the competition between the enhanced SHE and the shunting effect.

Upon increasing the strength of the Rashba parameter [Figs. 3(c) and 3(e)], the spin-to-charge and charge-to-spin conversion efficiencies become less sensitive to the spin diffusion length. Concomitantly, the spin-to-charge conversion (red lines) becomes progressively independent of the nonmagnetic metal conductivity [this is particularly clear in panel (e)], while the charge-to-spin conversion keeps on decreasing. In other words, in the case of dominant interfacial spin-orbit
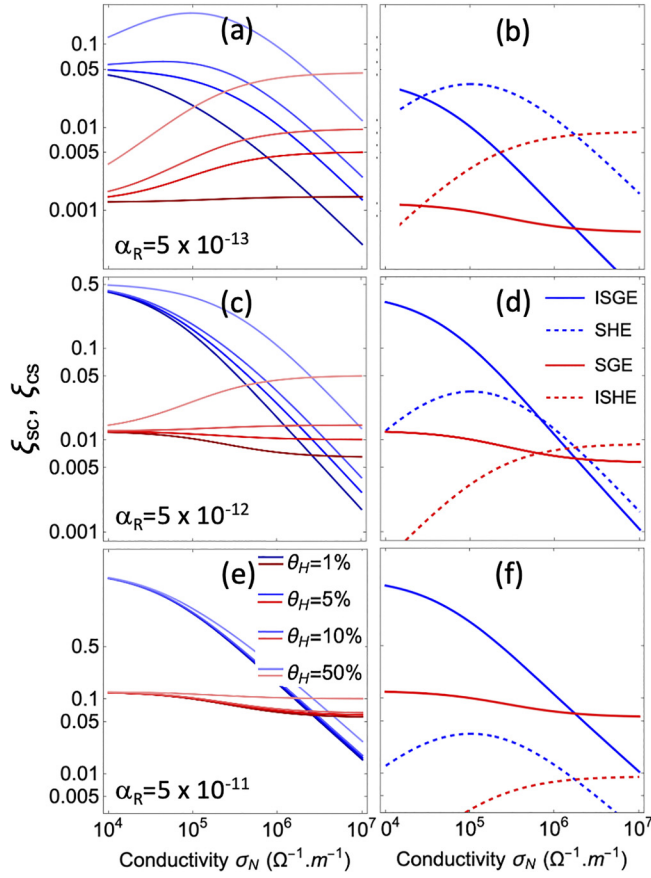
FIG. 3. Left panels: Spin-to-charge (red) and charge-to-spin (blue) conversion efficiencies for (a) weak, (c) intermediate, and (e) strong interfacial Rashba spin-orbit parameters for various values of the spin Hall angle. Right panels: Corresponding contributions of the spin Hall effect (SHE), inverse spin Hall effect (ISHE), interfacial spin galvanic effect (SGE), and inverse spin galvanic effect (ISGE), for $\theta_H = 10\%$. In all these calculations, we set $\lambda_N = 1$ nm.

coupling, the spin-to-charge conversion is much less sensitive to the spin current leakage than the charge-to-spin conversion. The decomposition of the conversion efficiencies in terms of SGE and SHE confirms this trend.

D. Extracting interfacial spin-charge interconversion coefficient from experiments

The spin-charge interconversion coefficients ξ_{sc} and ξ_{cs} are often used to extract the interfacial Rashba parameter, α_R. The extraction procedure requires the knowledge of basic transport properties such as conductivity, interfacial conductances, and spin diffusion lengths, but also relies on the scenario adopted. Assuming purely 2D transport, the Rashba parameter associated with charge-to-spin conversion reads

$$\frac{\alpha_R^{2D}}{\hbar} = \frac{\xi_{cs}}{2G_{\uparrow\downarrow}} \frac{\sigma_{2D}}{d_N + t_{2D}} \left(\frac{1}{\tau_{sf}} + \frac{1}{\tau_F} \right), \qquad (20)$$

and the parameter associated with spin-to-charge conversion reads

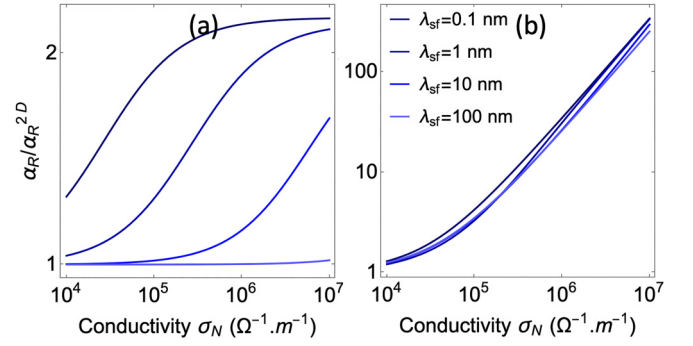$$\frac{\alpha_R^{2D}}{\hbar} = \frac{\xi_{sc}}{\tau_{sf}} (d_N + t_{2D}). \qquad (21)$$

FIG. 4. Ratios between the actual value of the Rashba parameter in a magnetic bilayer and its nominal when only interfacial transport is assumed, for (a) spin-to-charge and (b) charge-to-spin conversion experiments.

Now, assuming that transport is allowed in the neighboring metal, we obtain

$$\frac{\alpha_R}{\hbar} = \frac{\xi_{cs}}{2G_{\uparrow\downarrow}} \frac{\sigma_{2D} + \sigma_N d_N}{d_N + t_{2D}} \left(\frac{1}{\tau_{sf}} + \frac{1}{\tau_F} + \frac{1}{\tau_N} \frac{1}{1 + \eta_N} \right)$$
$$- \frac{1}{\tau_N} \frac{\tilde{\lambda}_N \tilde{\theta}_N}{1 + \eta_N}, \qquad (22)$$

for charge-to-spin conversion, and

$$\frac{\alpha_R}{\hbar} = \xi_{sc}(d_N + t_{2D}) \left(\frac{1}{\tau_{sf}} + \frac{1}{\tau_N} \frac{1}{1 + \eta_N} \right) - \frac{1}{\tau_N} \frac{\tilde{\lambda}_N \tilde{\theta}_N}{1 + \eta_N}, \qquad (23)$$

for spin-to-charge conversion. To assess how spin current leakage affects the extraction of the interfacial Rashba parameter, Fig. 4 shows the ratio α_R/α_R^{2D} as a function of the nonmagnetic metal conductivity for (a) spin-to-charge and (b) charge-to-spin conversion experiments. For these simulations, we assumed $\xi_{sc} = \xi_{cs} = 50\%$. Clearly, in the limit of an insulating nonmagnetic metal ($\sigma_N \to 0$), $\alpha_R \to \alpha_R^{2D}$, and in the limit of a highly conducting nonmagnetic metal, the extracted value of α_R increases substantially. Interestingly, spin-to-charge and charge-to-spin conversion lead to very different behaviors. When ξ_{sc} is used to quantify the Rashba parameter, the value of α_R saturates when $\eta_N \approx 1$. The maximum value obtained in (a) is about

$$\frac{\alpha_R}{\alpha_R^{2D}} \to 1 + (\tau_{sf}/\tau_N) \left(1 - \frac{\tilde{\lambda}_N \tilde{\theta}_N}{\xi_{sc}(d_N + t_{2D})} \right), \qquad (24)$$

which yields a saturation value of the order of 2.2 for our set of parameters. In contrast, using the charge-to-spin conversion efficiency ξ_{cs}, the extracted parameter is proportional to the conductivity of the nonmagnetic metal,

$$\frac{\alpha_R}{\alpha_R^{2D}} \to \frac{\sigma_N d_N}{\sigma_{2D}} \frac{\frac{1}{\tau_{sf}} + \frac{1}{\tau_F} + \frac{1}{\tau_N} \frac{1}{1 + \eta_N}}{\frac{1}{\tau_{sf}} + \frac{1}{\tau_F}}. \qquad (25)$$

Based on these observations, one can draw several conclusions. First, neglecting the potential spin current leakage and its associated SHE can lead to major discrepancies between the extracted interfacial Rashba parameter and the real one. A critical knob in the present theory is the spin transparency η_N.

The proper estimate of interfacial spin-charge interconversion requires the accurate determination of this coefficient, i.e., spin relaxation length and interfacial conductance. Finally, it is remarkable that the Rashba parameter extracted from spin-to-charge conversion experiments is much less sensitive to spin current leakage than when using charge-to-spin conversion experiments. This result suggests that spin-pumping is a better tool than spin-orbit torque for the extraction of the interfacial Rashba parameter.

IV. CONCLUSION

In order to solve controversial puzzles in spin-charge interconversion experiments, we have developed a phenomenological model that accounts for both interfacial SGE and bulk SHE effect. We find that when interfacial spin-charge interconversion is present, the leakage of spin current into the adjacent nonmagnetic metal substantially affects the overall spin-charge conversion efficiency, even in the absence of SHE. Most interestingly, the spin-to-charge and charge-to-spin conversions are affected differently: converting a charge current into a spin current is much more sensitive to the spin current absorption in the nonmagnetic metal due to the backflow associated with spin relaxation. In contrast, the charge current induced by a spin current is much more robust against spin current leakage.

This observation opens two interesting avenues. First, it clarifies the recent experimental reports on interconversion in topological insulators and explains why charge-to-spin conversion efficiencies tend to be orders of magnitude larger than spin-to-charge conversion efficiencies [20–33]. In addition, it also indicates that the value of the interfacial Rashba parameter extracted from spin pumping experiments are, *a priori*, much more trustable than values extracted from spin-orbit torque experiments.

[1] A. Manchon, J. Zelezný, I. M. Miron, T. Jungwirth, J. Sinova, A. Thiaville, K. Garello, and P. Gambardella, Current-induced spin-orbit torques in ferromagnetic and antiferromagnetic systems, Rev. Mod. Phys. **91**, 035004 (2019).

[2] W. Han, Y. C. Otani, and S. Maekawa, Quantum materials for spin and charge conversion, npj Quantum Mater. **3**, 27 (2018).

[3] T. Nan, D. C. Ralph, E. Y. Tsymbal, and A. Manchon, Emerging materials for spin-charge interconversion, APL Mater. **9**, 120401 (2021).

[4] K. Kondou and Y. Otani, Emergence of spin-charge conversion functionalities due to spatial and time-reversal asymmetries and chiral symmetry, Front. Phys. **11**, 1140286 (2023).

[5] E. Saitoh, M. Ueda, H. Miyajima, and G. Tatara, Conversion of spin current into charge current at room temperature: Inverse spin-Hall effect, Appl. Phys. Lett. **88**, 182509 (2006).

[6] O. Mosendz, J. E. Pearson, F. Y. Fradin, G. E. W. Bauer, S. D. Bader, and A. Hoffmann, Quantifying spin Hall angles from spin pumping: Experiments and theory, Phys. Rev. Lett. **104**, 046601 (2010).

[7] J.-C. Rojas-Sánchez, N. Reyren, P. Laczkowski, W. Savero, J.-P. Attane, C. Deranlot, M. Jamet, J.-M. George, L. Vila, and H. Jaffrès, Spin pumping and inverse spin Hall effect in platinum: The essential role of spin-memory loss at metallic interfaces, Phys. Rev. Lett. **112**, 106602 (2014).

[8] V. T. Pham, L. Vila, G. Zahnd, A. Marty, W. Savero-Torres, M. Jamet, and J. P. Attané, Ferromagnetic/nonmagnetic nanostructures for the electrical measurement of the spin Hall effect, Nano Lett. **16**, 6755 (2016).

[9] B. Heinrich, C. Burrowes, E. Montoya, B. Kardasz, E. Girt, Y.-Y. Song, Y. Sun, and M. Wu, Spin pumping at the magnetic insulator (YIG)/normal metal (Au) interfaces, Phys. Rev. Lett. **107**, 066604 (2011).

[10] C. Hahn, G. de Loubens, O. Klein, M. Viret, V. V. Naletov, and J. Ben Youssef, Comparative measurements of inverse spin Hall effects and magnetoresistance in YIG/Pt and YIG/Ta, Phys. Rev. B **87**, 174417 (2013).

[11] C. Hahn, G. de Loubens, M. Viret, O. Klein, V. V. Naletov, and J. Ben Youssef, Detection of microwave spin pumping using the inverse spin Hall effect, Phys. Rev. Lett. **111**, 217204 (2013).

[12] C. O. Avci, A. Quindeau, C.-F. Pai, M. Mann, L. Caretta, A. S. Tang, M. C. Onbasli, C. A. Ross, and G. S. D. Beach, Current-induced switching in a magnetic insulator, Nat. Mater. **16**, 309 (2017).

[13] P. Vaidya, S. A. Morley, J. V. Tol, Y. Liu, R. Cheng, A. Brataas, D. Lederman, and E. Barco, Subterahertz spin pumping from an insulating antiferromagnet, Science **368**, 160 (2020).

[14] J. Li, C. B. Wilson, R. Cheng, M. Lohmann, M. Kavand, and W. Yuan, Spin current from sub-terahertz-generated antiferromagnetic magnons, Nature (London) **578**, 70 (2020).

[15] A. Hoffmann, Spin Hall effects in metals, IEEE Trans. Magn. **49**, 5172 (2013).

[16] J. Sinova, S. O. Valenzuela, J. Wunderlich, C. H. Back, and T. Jungwirth, Spin Hall effect, Rev. Mod. Phys. **87**, 1213 (2015).

[17] J. C. Rojas-Sánchez, L. Vila, G. Desfonds, S. Gambarelli, J.-P. Attane, J. M. D. Teresa, C. Magén, and A. Fert, Spin-to-charge conversion using Rashba coupling at the interface between nonmagnetic materials, Nat. Commun. **4**, 2944 (2013).

[18] W. Zhang, M. B. Jungfleisch, W. Jiang, J. E. Pearson, and A. Hoffmann, Spin pumping and inverse Rashba-Edelstein effect in NiFe/Ag/Bi and NiFe/Ag/Sb, J. Appl. Phys. **117**, 17C727 (2015).

[19] S. Karube, K. Kondou, and Y. C. Otani, Experimental observation of spin-to-charge current conversion at non-magnetic metal/Bi$_2$O$_3$ interfaces, Appl. Phys. Express **9**, 033001 (2016).

[20] A. R. Mellnik, J. S. Lee, A. Richardella, J. L. Grab, P. J. Mintun, M. H. Fischer, A. Vaezi, A. Manchon, E.-A. Kim, N. Samarth, and D. C. Ralph, Spin-transfer torque generated by a topological insulator, Nature (London) **511**, 449 (2014).

[21] Y. Fan, P. Upadhyaya, X. Kou, M. Lang, S. Takei, Z. Wang, J. Tang, L. He, L.-T. Chang, M. Montazeri, G. Yu, W. Jiang, T. Nie, R. N. Schwartz, Y. Tserkovnyak, and K. L. Wang, Magnetization switching through giant spin-orbit torque in a magnetically doped topological insulator heterostructure, Nat. Mater. **13**, 699 (2014).

[22] P. Deorani, J. Son, K. Banerjee, N. Koirala, M. Brahlek, S. Oh, and H. Yang, Observation of inverse spin Hall effect in bismuth selenide, Phys. Rev. B **90**, 094403 (2014).

[23] Y. Shiomi, K. Nomura, Y. Kajiwara, K. Eto, M. Novak, K. Segawa, Y. Ando, and E. Saitoh, Spin-electricity conversion induced by spin injection into topological insulators, Phys. Rev. Lett. **113**, 196601 (2014).

[24] Y. Wang, P. Deorani, K. Banerjee, N. Koirala, M. Brahlek, S. Oh, and H. Yang, Topological surface states originated spin-orbit torques in Bi_2Se_3, Phys. Rev. Lett. **114**, 257202 (2015).

[25] M. Jamali, J. S. Lee, J. S. Jeong, F. Mahfouzi, Y. Lv, Z. Zhao, B. Nikolic, K. A. Mkhoyan, N. Samarth, and J.-P. Wang, Giant spin pumping and inverse spin Hall effect in the presence of surface spin-orbit coupling of topological insulator Bi_2Se_3, Nano Lett. **15**, 7126 (2015).

[26] H. Wang, J. Kally, J. S. Lee, T. Liu, H. Chang, D. R. Hickey, K. A. Mkhoyan, M. Wu, A. Richardella, and N. Samarth, Surface-state-dominated spin-charge current conversion in topological-insulator–ferromagnetic-insulator heterostructures, Phys. Rev. Lett. **117**, 076601 (2016).

[27] K. Kondou, R. Yoshimi, A. Tsukazaki, Y. Fukuma, J. Matsuno, K. S. Takahashi, M. Kawasaki, Y. Tokura, and Y. Otani, Fermi level dependent charge-to-spin current conversion by Dirac surface state of topological insulators, Nat. Phys. **12**, 1027 (2016).

[28] J. C. Rojas-Sánchez, S. Oyarzún, Y. Fu, A. Marty, C. Vergnaud, S. Gambarelli, L. Vila, M. Jamet, Y. Ohtsubo, A. Taleb-Ibrahimi, P. Le Fèvre, F. Bertran, N. Reyren, J. M. George, and A. Fert, Spin to charge conversion at room temperature by spin pumping into a new type of topological insulator: α-Sn films, Phys. Rev. Lett. **116**, 096602 (2016).

[29] Y. Wang, D. Zhu, Y. Wu, Y. Yang, J. Yu, R. Ramaswamy, R. Mishra, S. Shi, M. Elyasi, K. leong Teo, Y. Wu, and H. Yang, Room temperature magnetization switching in topological insulator-ferromagnet heterostructures by spin-orbit torques, Nat. Commun. **8**, 1364 (2017).

[30] D. Mahendra, R. Grassi, J. Y. Chen, M. Jamali, D. R. Hickey, D. Zhang, Z. Zhao, H. Li, P. Quarterman, Y. Lv, M. Li, A. Manchon, K. A. Mkhoyan, T. Low, and J. P. Wang, Room-temperature high spin-orbit torque due to quantum confinement in sputtered $Bi_xSe_{(1-x)}$ films, Nat. Mater. **17**, 800 (2018).

[31] H. Wu, P. Zhang, P. Deng, Q. Lan, Q. Pan, S. A. Razavi, X. Che, L. Huang, B. Dai, K. Wong, X. Han, and K. L. Wang, Room-temperature spin-orbit torque from topological surface states, Phys. Rev. Lett. **123**, 207205 (2019).

[32] F. Bonell, M. Goto, G. Sauthier, J. F. Sierra, A. I. Figueroa, M. V. Costache, S. Miwa, Y. Suzuki, and S. O. Valenzuela, Control of spin-orbit torques by interface engineering in topological insulator heterostructures, Nano Lett. **20**, 5893 (2020).

[33] H. He, L. Tai, H. Wu, D. Wu, A. Razavi, T. A. Gosavi, E. S. Walker, K. Oguz, C. C. Lin, K. Wong, Y. Liu, B. Dai, and K. L. Wang, Conversion between spin and charge currents in topological-insulator/nonmagnetic-metal systems, Phys. Rev. B **104**, L220407 (2021).

[34] Q. Shao, G. Yu, Y.-W. Lan, Y. Shi, M.-Y. Li, C. Zheng, X. Zhu, L.-J. Li, P. K. Amiri, and K. L. Wang, Strong Rashba-Edelstein effect-induced spin-orbit torques in monolayer transition metal dichalcogenide/ferromagnet bilayers, Nano Lett. **16**, 7514 (2016).

[35] D. MacNeill, G. M. Stiehl, M. H. D. Guimaraes, R. A. Buhrman, J. Park, and D. C. Ralph, Control of spin-orbit torques through crystal symmetry in WTe_2/ferromagnet bilayers, Nat. Phys. **13**, 300 (2017).

[36] S. Shi, S. Liang, Z. Zhu, K. Cai, S. D. Pollard, Y. Wang, J. Wang, Q. Wang, P. He, J. Yu, G. Eda, G. Liang, and H. Yang, All-electric magnetization switching and Dzyaloshinskii-Moriya interaction in WTe_2/ferromagnet heterostructures, Nat. Nanotechnol. **14**, 945 (2019).

[37] F. Xue, C. Rohmann, J. Li, V. Amin, and P. Haney, Unconventional spin-orbit torque in transition metal dichalcogenide-ferromagnet bilayers from first-principles calculations, Phys. Rev. B **102**, 014401 (2020).

[38] Q. Xie, W. Lin, S. Sarkar, X. Shu, S. Chen, L. Liu, T. Zhao, C. Zhou, H. Wang, J. Zhou, S. Gradečak, and J. Chen, Field-free magnetization switching induced by the unconventional spin-orbit torque from WTe_2, APL Mater. **9**, 051114 (2021).

[39] W. S. Torres, J. F. Sierra, L. A. Benítez, F. Bonell, M. V. Costache, and S. O. Valenzuela, Spin precession and spin Hall effect in monolayer graphene/Pt nanostructures, 2D Mater. **4**, 041008 (2017).

[40] C. K. Safeer, N. Ontoso, J. Ingla-Aynés, F. Herling, V. T. Pham, A. Kurzmann, K. Ensslin, A. Chuvilin, I. Robredo, M. G. Vergniory, F. D. Juan, L. E. Hueso, M. R. Calvo, and F. Casanova, Large multidirectional spin-to-charge conversion in low-symmetry semimetal $MoTe_2$ at room temperature, Nano Lett. **19**, 8758 (2019).

[41] L. A. Benítez, W. S. Torres, J. F. Sierra, M. Timmermans, J. H. Garcia, S. Roche, M. V. Costache, and S. O. Valenzuela, Tunable room-temperature spin galvanic and spin Hall effects in van der Waals heterostructures, Nat. Mater. **19**, 170 (2020).

[42] I. Shin, W. J. Cho, E. S. An, S. Park, H. W. Jeong, S. Jang, W. J. Baek, S. Y. Park, D. H. Yang, J. H. Seo, G. Y. Kim, M. N. Ali, S. Y. Choi, H. W. Lee, J. S. Kim, S. D. Kim, and G. H. Lee, Spin-orbit torque switching in an all-van der Waals heterostructure, Adv. Mater. **34**, 2101730 (2022).

[43] Q. Xie, W. Lin, J. Liang, H. Zhou, M. Waqar, M. Lin, S. L. Teo, H. Chen, X. Lu, X. Shu, L. Liu, S. Chen, C. Zhou, J. Chai, P. Yang, K. P. Loh, J. Wang, W. Jiang, A. Manchon, H. Yang *et al.*, Rashba-Edelstein effect in the h-BN van der Waals interface for magnetization switching, Adv. Mater. **34**, 2109449 (2022).

[44] W. Y. Choi, I. C. Arango, V. T. Pham, D. C. Vaz, H. Yang, I. Groen, C. C. Lin, E. S. Kabir, K. Oguz, P. Debashis, J. J. Plombon, H. Li, D. E. Nikonov, A. Chuvilin, L. E. Hueso, I. A. Young, and F. Casanova, All-electrical spin-to-charge conversion in sputtered Bi_xSe_{1-x}, Nano Lett. **22**, 7992 (2022).

[45] N. Ontoso, C. K. Safeer, F. Herling, J. Ingla-Aynés, H. Yang, Z. Chi, B. Martin-Garcia, I. Robredo, M. G. Vergniory, F. de Juan, M. Reyes Calvo, L. E. Hueso, and F. Casanova, Unconventional charge-to-spin conversion in graphene/$MoTe_2$ van der Waals heterostructures, Phys. Rev. Appl. **19**, 014053 (2023).

[46] E. Lesne, Y. Fu, S. Oyarzun, J. C. Rojas-Sánchez, D. C. Vaz, H. Naganuma, G. Sicoli, J. P. Attané, M. Jamet, E. Jacquet, J. M. George, A. Barthélémy, H. Jaffrès, A. Fert, M. Bibes, and L. Vila, Highly efficient and tunable spin-to-charge conversion

through Rashba coupling at oxide interfaces, Nat. Mater. **15**, 1261 (2016).

[47] Y. Wang, R. Ramaswamy, M. Motapothula, K. Narayanapillai, D. Zhu, J. Yu, T. Venkatesan, and H. Yang, Room-temperature giant charge-to-spin conversion at the $SrTiO_3$-$LaAlO_3$ oxide interface, Nano Lett. **17**, 7659 (2017).

[48] D. C. Vaz, P. Noël, A. Johansson, B. Göbel, F. Y. Bruno, G. Singh, S. McKeown-Walker, F. Trier, L. M. Vicente-Arche, A. Sander, S. Valencia, P. Bruneel, M. Vivek, M. Gabay, N. Bergeal, F. Baumberger, H. Okuno, A. Barthélémy, A. Fert, L. Vila *et al.*, Mapping spin-charge conversion to the band structure in a topological oxide two-dimensional electron gas, Nat. Mater. **18**, 1187 (2019).

[49] F. Trier, D. C. Vaz, P. Bruneel, P. Noe, A. Fert, L. Vila, J. Philippe Attane, A. Barthelemy, M. Gabay, H. Jaffres, and M. Bibes, Electric-field control of spin current generation and detection in ferromagnet-free $SrTiO_3$-based nanodevices, Nano Lett. **20**, 395 (2020).

[50] F. Gallego, F. Trier, S. Mallik, J. Bréhin, S. Varotto, L. M. Vicente-Arche, T. Gosavy, C. C. Lin, J. R. Coudevylle, L. Iglesias, F. Casanova, I. Young, L. Vila, J. P. Attané, and M. Bibes, All-electrical detection of the spin-charge conversion in nanodevices based on $SrTiO_3$ 2-D electron gases, Adv. Funct. Mater. **34**, 2307474 (2023).

[51] F. Trier, P. Noël, J. V. Kim, J. P. Attané, L. Vila, and M. Bibes, Oxide spin-orbitronics: Spin-charge interconversion and topological spin textures, Nat. Rev. Mater. **7**, 258 (2022).

[52] F. Calavalle, M. Suárez-Rodríguez, B. Martín-García, A. Johansson, D. C. Vaz, H. Yang, I. V. Maznichenko, S. Ostanin, A. Mateo-Alonso, A. Chuvilin, I. Mertig, M. Gobbi, F. Casanova, and L. E. Hueso, Gate-tuneable and chirality-dependent charge-to-spin conversion in tellurium nanowires, Nat. Mater. **21**, 526 (2022).

[53] P. Noël, F. Trier, L. M. V. Arche, J. Bréhin, D. C. Vaz, V. Garcia, S. Fusil, A. Barthélémy, L. Vila, M. Bibes, and J.-P. Attané, Non-volatile electric control of spin-charge conversion in a $SrTiO_3$ Rashba system, Nature (London) **580**, 483 (2020).

[54] S. Varotto, L. Nessi, S. Cecchi, J. Sławińska, P. Noël, S. Petrò, F. Fagiani, A. Novati, M. Cantoni, D. Petti, E. Albisetti, M. Costa, R. Calarco, M. B. Nardelli, M. Bibes, S. Picozzi, J. P. Attané, L. Vila, R. Bertacco, and C. Rinaldi, Room-temperature ferroelectric switching of spin-to-charge conversion in germanium telluride, Nat. Electron. **4**, 740 (2021).

[55] C. Rinaldi, S. Varotto, M. Asa, J. Sławińska, J. Fujii, G. Vinai, S. Cecchi, D. D. Sante, R. Calarco, I. Vobornik, G. Panaccione, S. Picozzi, and R. Bertacco, Ferroelectric control of the spin texture in GeTe, Nano Lett. **18**, 2751 (2018).

[56] G. Bihlmayer, P. Noël, D. V. Vyalikh, E. V. Chulkov, and A. Manchon, Rashba-like physics in condensed matter, Nat. Rev. Phys. **4**, 642 (2022).

[57] E. L. Ivchenko and G. E. Pikus, New photogalvanic effect in gyrotropic crystals, JETP Lett. **27**, 604 (1978).

[58] F. Vasko, Spin splitting in the spectrum of two-dimensional electrons due to the surface potential, JETP Lett. **30**, 541 (1979).

[59] V. M. Edelstein, Spin polarization of conduction electrons induced by electric current in two-dimensional asymmetric electron systems, Solid State Commun. **73**, 233 (1990).

[60] S. Zhang and A. Fert, Conversion between spin and charge currents with topological insulators, Phys. Rev. B **94**, 184423 (2016).

[61] R. Dey, N. Prasad, L. F. Register, and S. K. Banerjee, Conversion of spin current into charge current in a topological insulator: Role of the interface, Phys. Rev. B **97**, 174406 (2018).

[62] H. Isshiki, P. Muduli, J. Kim, K. Kondou, and Y. C. Otani, Phenomenological model for the direct and inverse Edelstein effects, Phys. Rev. B **102**, 184411 (2020).

[63] E. G. Mishchenko, A. V. Shytov, and B. I. Halperin, Spin current and polarization in impure two-dimensional electron systems with spin-orbit coupling, Phys. Rev. Lett. **93**, 226602 (2004).

[64] A. A. Burkov, Theory of spin-charge-coupled transport in a two-dimensional electron gas with Rashba spin-orbit interactions, Phys. Rev. B **70**, 155308 (2004).

[65] W.-G. Wang, M. Li, S. Hageman, and C. L. Chien, Electric-field-assisted switching in magnetic tunnel junctions, Nat. Mater. **11**, 64 (2012).

[66] A. Brataas, Y. Tserkovnyak, G. E. W. Bauer, and P. J. Kelly, Spin pumping and spin transfer, in *Spin Current* (Oxford University Press, New York, 2012).

[67] M. Zwierzycki, Y. Tserkovnyak, P. J. Kelly, A. Brataas, and G. E. W. Bauer, First-principles study of magnetization relaxation enhancement and spin transfer in thin magnetic films, Phys. Rev. B **71**, 064420 (2005).

[68] A. Brataas, G. E. W. Bauer, and P. Kelly, Non-collinear magnetoelectronics, Phys. Rep. **427**, 157 (2006).